SIMULATION STUDY ON TRANSPORT CHARACTERISTICS OF LEAKAGE GAS FROM THE CONDENSER OF POWER PLANT

Wenyan Bi [1]***, Qiang Zhou*** [1]***, Jianfeng Wan*** [2*]***, Xiangxuan Xu*** [2]***, Jian Hu*** [2]***, Menglin Yu*** [2]***, Yihong Sun*** [2]***, Yikai Hou*** [1]***, Xuemao Guan*** [3*]

[1]College of Chemistry and Chemical Engineering, Henan Polytechnic University, Jiaozuo, Henan 454000, China;

[2]School of Mechanical and Power Engineering, Henan Polytechnic University, Jiaozuo, Henan 454000, China;

[3]School of Materials Science and Engineering, Henan Polytechnic University, Jiaozuo, Henan 454000, China

* Jianfeng Wan; E-mail: wanjianfeng@hpu.edu.cn
* Xuemao Guan; E-mail: guanxuemao@hpu.edu.cn

Exploring the transport characteristics of leakage gas in the condenser can facilitate quicker identification of leak points when using Helium tracer gas method for detection. We construct a three-dimensional physical model of the condenser to simulate the Helium gas leakage process within the tube bundle. On the steam side, we adopt RNG $k-\varepsilon$, porous media, steam condensation, and convective diffusion models to describe steam and leakage gas flow. On the waterside, we use the tube bundle thermal resistance model to describe the steam-water heat transfer. The research concludes with three key points. When the centripetal pressure gradient is insufficient, there will be leakage gas enrichment, resulting in flowing out in the form of diffusion. When there is no centripetal pressure gradient in the tube bundle region, it will extract only a small amount of upstream leakage gas along with steam through the flow. When reaching a stable level for leakage gas, the leakage intensity is proportional to the outlets' flow rate but is independent of the transport form. The deviation of the mass flow rate decreases with the mesh quantity increasing, which is less than 2% when the mesh quantity is over 638228. The deviation between simulated and actual values of the two parameters is less than 5%, which reveals the good agreement between numerical calculation and actual work conditions. These conclusions can assist employees and researchers in evaluating data on leak points and enhancing detection techniques.

Key words*: Steam condenser, Tube bundle leakage, Porous media, Tracer gas transport, Flow simulation*

1 Introduction

The steam condenser is an essential component of the turbine system in power plants [1, 2]. It cools the turbine and steam by circulating water within the tube bundle to form and maintain a specific vacuum level at the turbine exhaust outlet. The performance of this equipment directly affects the economic efficiency and reliability of the turbine generator [3, 4]. The condenser consists of the steam-side vacuum system and the water-side. The gas tightness is crucial for operation safety and generator efficiency [5, 6]. When the condenser water side has poor gas tightness, coupled with the close vacuum inside the condenser, it will cause the circulating water to leak because of the significantly higher pressure exerted by the circulating water compared to that inside the condenser. It will also affect feedwater quality, scale the boiler's heating surface, and potentially cause severe accidents, such as tube bursting [7, 8]. Therefore, it is essential to research the condenser's leakage detection techniques and prevention methods.

There are many available methods for leakage detection in tube bundles, such as ultrasonic detection [9], eddy-current testing [10], hydrostatic testing [11], and so on. Traditional condenser leakage detection methods require the machine shutdown, which is time-consuming and resource-consuming, and directly affects the economic efficiency of power plants [12, 13]. Now, there is a condenser tube bundle detection method based on Helium tracer gas that can avoid these issues [14, 15]. The detection method involves closing the circulating water in the tube bundle and injecting Helium tracer gas into the predetermined tube bundle. In case of any leaks, Helium would migrate to the steam side of the condenser through the hole and be extracted along with the uncondensed gas. By measuring the content of the tracer gas at the extraction port, it is possible to infer if there is a leak. However, there is little research on establishing the relationship between leakage gas flow rate and operating conditions. Therefore, conducting in-depth research on the transport characteristics of leakage gas is essential.

To investigate the transport rules and locate the leak point faster, this paper presents a numerical model for tube bundle and fluid regions in the power plant's condenser. According to the power plant's actual operating conditions, a tracer gas (Helium) is introduced to simulate leaks occurring at predetermined locations within the tube bundle. The simulation includes an analysis of internal flow field distribution and mass flow rate at extraction ports to examine Helium leakage behavior under various operating conditions.

2 Methodology

2.1 Physical model and numerical meshes

Fig. 1 shows the three-dimensional physical model of the condenser. It consists of two chambers, each with two extraction ports, labelled as Port 1#, 2#, 3#, and 4#. The condenser's internal structure is complex and can be divided into the tube bundle and fluid regions. The green arrows in the figure indicate the tube bundle zones, which are approximately rectangular. Four tube bundle zones are along the X-axis, labelled as Zone 1, 2, 3, and 4. Each tube bundle zone is equipped with an extraction turbine and a circulating water pump at center. Specifically, Ports 1# and 3# share one extraction turbine and circulating water pump, while Ports 2# and 4# also share another extraction turbine and circulating water pump. Therefore, the extraction turbine and circulating water pump in Zones 1 and 3 must be opened or closed simultaneously, and the same applies to Zones 2 and 4. The direct

calculation is nearly impossible since the condenser has thousands of heat exchange tubes. Hence this article simplifies the tube bundle zone using a porous media model, while all other areas outside the tube bundle zone are considered as fluid regions.

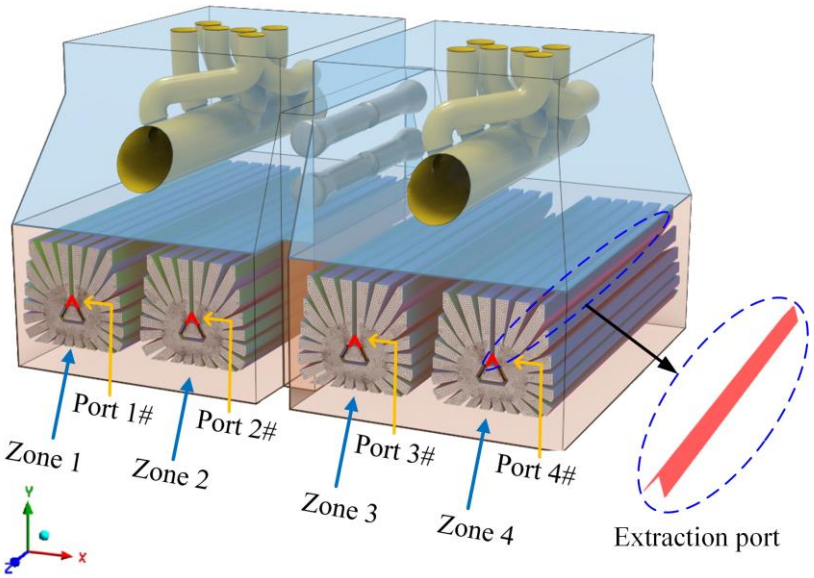

Fig. 1 Three-dimensional physical model of the condenser.

The convergence of the calculation results is influenced by the complexity of the flow field, thus necessitating a finer mesh division to ensure optimal mesh quality. We first establish a two-dimensional mesh. After achieving the stable and correct calculation, the three-dimensional mesh is subsequently constructed. Specifically, tetrahedral mesh is utilized in the condenser throat. In other areas, quadrilateral meshes are employed in the XY plane, followed by sweeping in the Z-direction to form hexahedral meshes. Since the flow velocity in the Z-direction is extremely low, only 12 meshes are allocated in that direction. According to practical experience, the maximum flow velocity is mainly concentrated in areas affected by steam, such as near the wall of various pipes in the throat area, between cooling bundles, and close to the extraction port. To better characterize the flow, these specific regions undergo individual refinement with encrypted meshes.

To verify the mesh independence, use four different sizes of meshes (473520, 534633, 638228, 721352) to conduct steady-state calculations. These calculations were performed under operating conditions No. 5 as indicated in tab. 1. The mass flow rate of steam at the extraction port was calculated for each mesh size and plotted in fig. 2. According to fig. 2, the deviation of the mass flow rate decreases with the mesh size increase, which is less than 2% when mesh sizes are 638228 and 721352. Considering the computational efficiency, this paper employs a mesh size of 638228 for subsequent simulations.

Tab. 1 Basic working conditions of condenser.

NO.	Operating loads (MW)	Mass flow rate in the condenser inlet (kg/s)	Cooling water temperature (℃)	Condenser back pressure (KPa)	Circulating water pump opening conditions
1	600	220.209	10	6.7	single-row
2	600	238.487	24	3.3	single-row
3	840	295.550	10	8.4	single-row
4	840	317.408	24	4.3	single-row
5	100% TMCR	371.782	24	5.6	double-row

Note: “TMCR” represents the turbine's maximum continuous rate.

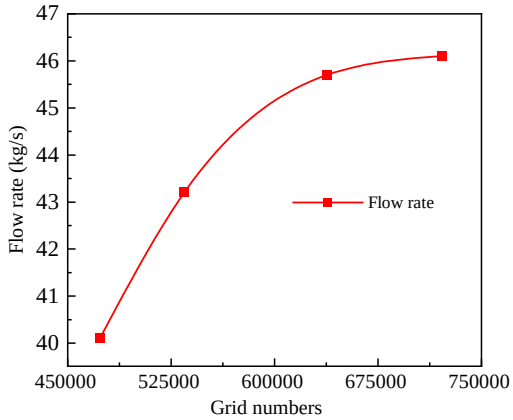

Fig. 2 Mesh independence verification diagram.

2.2 Numerical model

2.2.1 Governing equations

To simulate the internal flow field and mass transfer in the condenser, a set of governing equations (Eqs. (1) ~ (8)) are established to describe the transient flow. The equations can be divided into three parts: the steam mass conservation equation (Eq. (1)), the momentum equation for the mixture (Eqs. (2) ~ (4)), and the convective-diffusion equation for Helium (Eq. (5)). The parameters β and c_a are the constants. The unknown variables of F_x, F_y, F_z and $\dot{m}$ are determined by Eqs. (6) ~ (9). Additionally, there are six other unknown variables (ρ, p, u, v, w, x_a). To make the equations close, we introduce the ideal gas state equation.

$$\frac{\partial(\beta\rho)}{\partial t}+\frac{\partial(\beta\rho u)}{\partial x}+\frac{\partial(\beta\rho v)}{\partial y}+\frac{\partial(\beta\rho w)}{\partial z}=-\dot{m} \tag{1}$$

$$\begin{aligned}&\frac{\partial(\beta\rho u)}{\partial t}+\frac{\partial(\beta\rho uu)}{\partial x}+\frac{\partial(\beta\rho vu)}{\partial y}+\frac{\partial(\beta\rho wu)}{\partial z}\\&=\frac{\partial}{\partial x}\left(\beta\mu\frac{\partial u}{\partial x}\right)+\frac{\partial}{\partial y}\left(\beta\mu\frac{\partial u}{\partial y}\right)+\frac{\partial}{\partial z}\left(\beta\mu\frac{\partial u}{\partial z}\right)-\beta\frac{\partial p}{\partial x}-\beta F_x\\&-\dot{m}u\end{aligned} \tag{2}$$

$$\begin{aligned}&\frac{\partial(\beta\rho v)}{\partial t}+\frac{\partial(\beta\rho uv)}{\partial x}+\frac{\partial(\beta\rho vv)}{\partial y}+\frac{\partial(\beta\rho wv)}{\partial z}\\&=\frac{\partial}{\partial x}\left(\beta\mu\frac{\partial v}{\partial x}\right)+\frac{\partial}{\partial y}\left(\beta\mu\frac{\partial v}{\partial y}\right)+\frac{\partial}{\partial z}\left(\beta\mu\frac{\partial v}{\partial z}\right)-\beta\frac{\partial p}{\partial y}-\beta F_y\\&-\dot{m}v\end{aligned} \tag{3}$$

$$\begin{aligned}&\frac{\partial(\beta\rho v)}{\partial t}+\frac{\partial(\beta\rho uw)}{\partial x}+\frac{\partial(\beta\rho vw)}{\partial y}+\frac{\partial(\beta\rho ww)}{\partial z}\\&=\frac{\partial}{\partial x}\left(\beta\mu\frac{\partial w}{\partial x}\right)+\frac{\partial}{\partial y}\left(\beta\mu\frac{\partial w}{\partial y}\right)+\frac{\partial}{\partial z}\left(\beta\mu\frac{\partial w}{\partial z}\right)-\beta\frac{\partial p}{\partial z}-\beta F_z\\&-\dot{m}w\end{aligned} \tag{4}$$

$$\frac{\partial(\beta\rho x_a)}{\partial t}+\frac{\partial(\beta\rho u x_a)}{\partial x}+\frac{\partial(\beta\rho v x_a)}{\partial y}+\frac{\partial(\beta\rho w x_a)}{\partial z} = \frac{\partial}{\partial x}\left(\beta c_a \frac{\partial x_a}{\partial x}\right)+\frac{\partial}{\partial y}\left(\beta c_a \frac{\partial x_a}{\partial y}\right)+\frac{\partial}{\partial z}\left(\beta c_a \frac{\partial x_a}{\partial z}\right)-M_a \quad (5)$$

where β represents the porosity [16], and the value of β is the ratio of fluid volume within the control body to the volume of the control body, which is determined by the tube bundle size and distribution. ρ represents the steam density. u, v, and w denote the flow velocities in the x, y, and z directions. $\dot{m}$ is the condensation rate of steam per unit volume. c_a is the diffusion coefficient of Helium [17]. x_a is the mass concentration of the leakage gas. M_a is the Helium mass sink, which remains zero everywhere except at the leak point. In this paper, the inlet steam flow velocity can reach more than 60 m/s. For the throat, because there is a complex tube bundle structure, most researchers adopt turbulence models to simulate steam flow [18]. The dynamic viscosity μ in Eqs. (2) ~ (4) consists of two parts, one is laminar dynamic viscosity and the other part is generated by turbulence, which is calculated by the RNG $k-\varepsilon$ model [19, 20].

From Eq. (5), there are two transport modes for Helium. One is the flow along with the steam, given by $\frac{\partial(\beta\rho u x_a)}{\partial x}+\frac{\partial(\beta\rho v x_a)}{\partial y}+\frac{\partial(\beta\rho w x_a)}{\partial z}$, where the transport velocity is consistent with the steam velocity. The other mode is diffusion caused by concentration difference, given by $\frac{\partial}{\partial x}\left(\beta c_a \frac{\partial x_a}{\partial x}\right)+\frac{\partial}{\partial y}\left(\beta c_a \frac{\partial x_a}{\partial y}\right)+\frac{\partial}{\partial z}\left(\beta c_a \frac{\partial x_a}{\partial z}\right)$. The transport velocity depends on Helium's concentration and diffusion coefficient.

$$F_x = \xi\rho u U_p \quad (6)$$

$$F_y = \xi\rho v U_p \quad (7)$$

$$F_z = \xi\rho w U_p \quad (8)$$

where F_x, F_y, and F_z represent the flow resistance of the mixed gas in the x, y, and z directions, respectively. ξ is the parameter related to the distribution of the bundle structure and the direction of the gas flow, which can be explicitly calculated by referring to the literature [21]. And U_p represents the magnitude of velocity, which is equal to the square root of the square sum of velocities in the three directions.

Condensation rate equation [22]:

$$\dot{m} = \frac{\Delta t_m C_A}{R_{tot}\gamma C_V} \quad (9)$$

where Δt_m is the logarithmic average temperature difference. R_{tot} is the total thermal resistance from the steam side to the waterside. γ is the latent heat of the local steam condensation. C_V and C_A are the control body thermal volume and cooling tube heat-transfer area, respectively.

According to the ideal gas state equation [23], the steam density ρ is :

$$\rho = \frac{p}{RT} \quad (10)$$

where R is the steam gas constant, and T is the stream gas temperature.

2.2.2 Boundary conditions

The boundary conditions for condenser calculation are composed of three parts: the inlet, outlet, and leak point part (fig. 3). Fig. 3a illustrates the distribution of steam inlet and outlet parts. The blue area represents the fluid inlet, and the dark red area represents the fluid outlet. These positions are labelled as Inlet 1, Inlet 2, Outlet 1, Outlet 2, Outlet 3, and Outlet 4 along the positive X-axis direction. The fluid outlet involves an area within 0~15 m along the Z-axis. To improve the computational stability, the inlet velocity adopts "the mass flow rate", while the outlet part adopts the "outflow" type. Considering the computational complexity and the analysis time, only one leak position is selected for investigation (fig. 3b). The leak point is located in Zone 4 (highlighted in red in fig. 3b), with a corresponding volume of 0.00894 m^3.

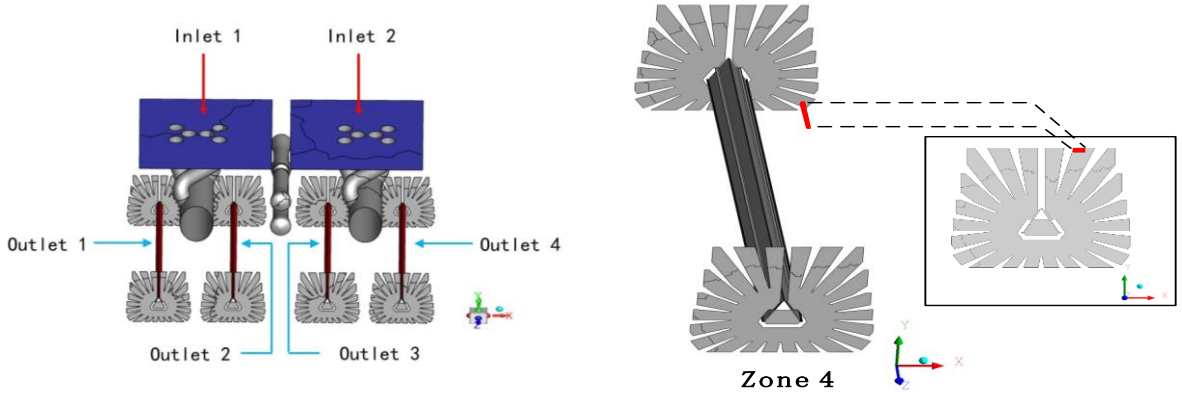

(a) Inlet and outlet positions (b) Schematic diagram of leakage point position

Fig. 3 Boundary conditions.

According to the above calculation methods and conditions, the RNG $k-\varepsilon$ turbulence model [24] is used for steady-state simulation. The near wall function adopts the standard wall function. The obtained steady-state simulation results are used as the initial conditions for transient simulation. The time step is set as 0.015 s, with a maximum iteration of 50 per unit time step.

The parameters for simulation are based on the NO.5 operating condition in Tab. 1. According to the simulation results, the calculated outlet steam gas temperature is 34.81 ℃, and the pressure is 3434.7 Pa, while corresponding values from the on-site data of the power plant under identical conditions are 35.01 ℃ and 3466.0 Pa, respectively. The deviation between simulated and actual values of the two parameters is less than 5%, which reveals the good agreement between numerical calculation and actual work conditions. Therefore, the effectiveness of the numerical simulation results is validated.

3 Simulation results and analysis

3.1 Transport characteristics of leakage gas under 600 MW and 840 MW

The simulation when the leakage intensity is 0.0779 kg/(m^3· s) is conducted based on the two operating loads of 600 MW (NO. 2) and 840 MW (NO. 4) in Tab. 1. Fig. 4 illustrates the relation between the leakage gas flow rate and time under different operating conditions. From figs. 4a and 4b, it can be observed that the Helium mass flow rates at Outlets 1 and 2 consistently remain at 0 kg/s. This indicates that gas leakage only occurs in the right chamber because it is separate from the left

chamber. Consequently, there is no mass flow rate at the extraction port of the left chamber, resulting in a value of 0 kg/s. In addition, despite the leak point located above Port 4#, Outlet 3 exhibits a significantly higher mass flow rate than Outlet 4.

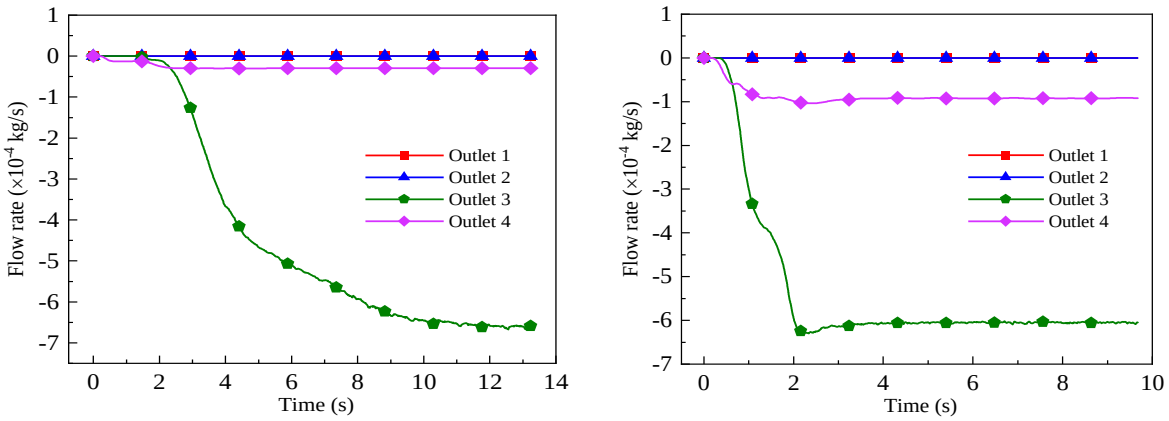

Fig. 4 Comparison diagram of leakage gas outlet flow rate under (a) 600 MW and (b) 840 MW when the circulating water pumps 1 and 3 are opened.

According to fig. 4, the flow rate at all outlets is almost stable after 3s when the operating load is 840 MW, while Outlet 4 under the operating load of 600 MW has not yet reached a stable level.

To analyze the reasons for the large flow rate difference between Outlet 3 and Outlet 4, depict the pressure and streamline cloud diagrams (fig. 5) under 840 MW after reaching steady. From fig. 5a, a large pressure gradient formed at Ports 1# and 3# when circulating water pumps 1 and 3 are opened. Since the centripetal pressure gradient is the main driving force for gas leakage from the extraction port, the gas from the leakage point in Zone 4 on the right chamber quickly enters Outlet 3. Conversely, due to the closure of circulating water pumps 2 and 4, no centripetal pressure gradient can be formed in the cooling area of Zones 2 and 4 (fig. 5a). The obvious pressure gradient is only found near Ports 2# and 4#. Combining to fig. 5a, there is no centripetal pressure gradient in the cooling area of Zones 2 and 4 in fig. 5b, leading to very few streamlines. Only a small amount of steam rushes into the extraction port from the inlet above and is taken away. Most streamlines flow from top to bottom along both sides of the cooling area of Zones 2 and 4. As shown in fig. 5b, leakage gas on the right side flows into the cooling area within Zones 1 and 3 along the ‘L’-shape path indicated by the red line in fig. 5b and then is extracted. Therefore, the mass flow rate of Outlet 3 is much higher than that of Outlet 4. It is worth noting that the leakage point studied is in Outlet 4 upstream, so a small part of the flow enters Outlet 4. But if the leakage point is not in Outlet 4 upstream, then no flow will enter Outlet 4, resulting in the flow rate being 0kg/s at Outlet 4.

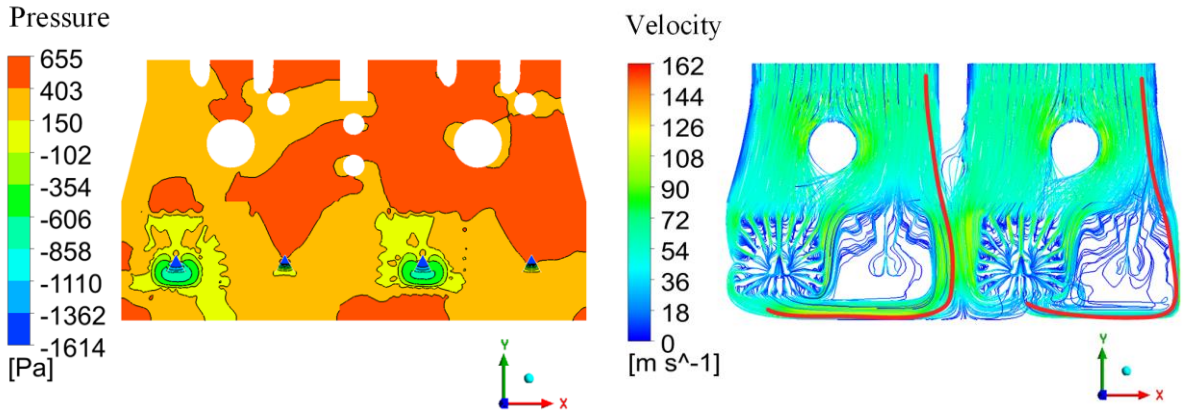

(a) (b)

Fig. 5 Cloud diagrams of pressure (a) and streamline (b) under 840 MW.

To further analyze the prolonged time required for the leakage gas flow to stabilize at Outlet 3 when the operating load is 600 MW (fig. 4a), the mass fraction diagrams of the leakage gas at 3s and 6s are drawn (fig. 6) and the mass distribution of the leakage gas is studied. Fig. 6a shows that the maximum mass fraction at Port 3# is 0.1, but it is nearly 0 at Port 4#. This suggests that the leakage gas at Port 4# has been extracted, while the gas at Port 3# has not been extracted and remains inside the extraction port to form an enrichment phenomenon. Fig. 6b shows that the maximum mass fraction of Port 3# at 6s is 0.127, which exceeds the value at 3s. This indicates that the enrichment phenomenon of leakage gas at Port 3# is intensified. On the other hand, the maximum mass fraction of Port 4# at 6s has not changed and remains close to 0.

In comparison, the time required for the flow rate of Outlet 3 to reach a stable level in fig. 4a is much longer than that in fig. 4b. This discrepancy can be attributed to the decrease in operation load from 840 MW to 600 MW, resulting in reduced steam. However, the quantity and temperature of circulating water remain unchanged. In this way, under the same cooling conditions, the cooling effect of low steam volume is better. It leads to part of the cooling area reaching a high vacuum level. The leakage gas entering the vacuum region cannot be extracted due to insufficient centripetal pressure gradient, causing enrichment. When enriched for a period of time, it will diffuse to the outlet through the concentration difference. Therefore, there are two stages in the transport process for leakage gas at Port 3# under 600 MW. In the first stage, the leakage gas flows along with the steam and reaches the extraction port. Some leakage gas leaves Port 3# due to the pressure gradient, while the remaining leakage gas will stay and enrich. In the second stage, the enriched leakage gas finally diffuses out of the extraction port through concentration difference. Since the time of the second stage is much longer than that of the first stage, the time required for Outlet 3 to reach the stable level at 600 MW in fig. 4 is significantly longer than that of other outlets.

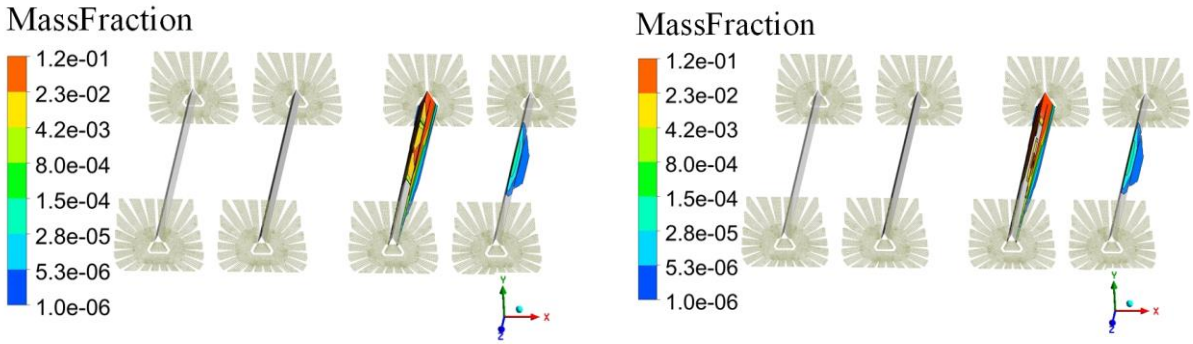

(a) (b)

Fig. 6 Mass fraction diagrams of the leakage gas inside the condenser at (a) 3s and (b) 6s under 600 MW.

From the above, the leakage gas flow rate change over time exhibits two fundamental forms, as illustrated in fig. 7a and fig. 7b. If the gas undergoes multiple flow and diffusion processes, the leakage gas transport mode will be a combination of these two forms.

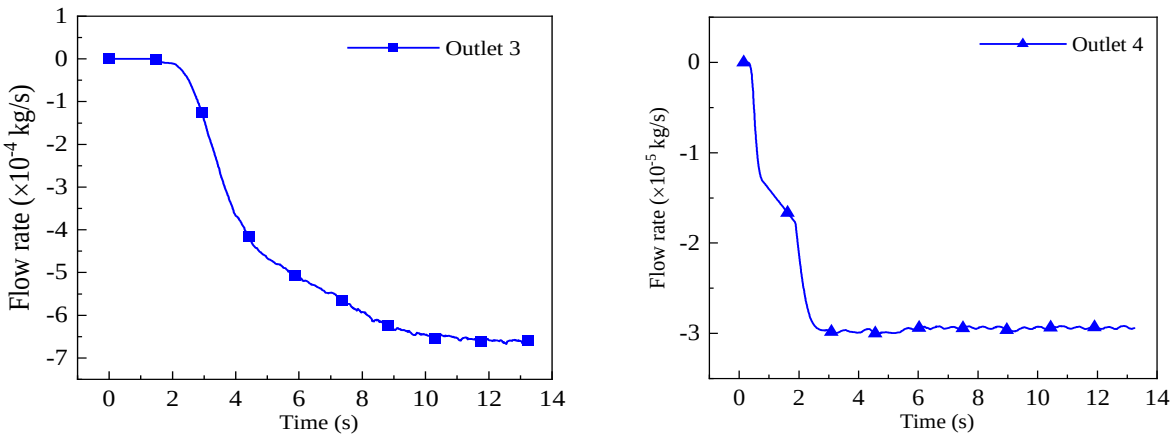

(a) (b)

Fig. 7 The outlet flow rate for both forms of leakage gas varied with time.

3.2 Transport rules under different leakage intensities

The leakage gas transport rules under different leakage intensities are investigated (tab. 2). The intensity values follow a specific proportional relationship (16:4:1). The leakage position in this section is also located above Zone 4 in the tube bundle area. Other operating conditions are set according to section 3.1. The transient simulation is conducted under different Helium leakage intensities.

Tab. 2 Leakage intensity table in different cases.

Case	Helium leakage intensity (kg/(m^3· s))
1	0.3110
2	0.0779
3	0.0194

Fig. 8 depicts the evolution curves of the outlet flow rate for leakage gas at three different leakage intensities. From an overall perspective, the trend of flow rate variation and the time required to reach

the stable level is almost the same among the three leakage intensities. The average flow rate of leakage gas at Outlet 4 accounted for around 12.3% of the total flow rate, while the average flow rate of leakage gas at Outlet 3 accounted for about 87.7% of the total flow rate. It indicates that changes in leakage intensity do not impact the steam flow. However, the specific values of the outlet flow rate are different for various leakage intensities. Through calculations, it is determined that there exists a proportional relationship between the outlet flow rates (16:4:1), which correspond to leakage intensities.

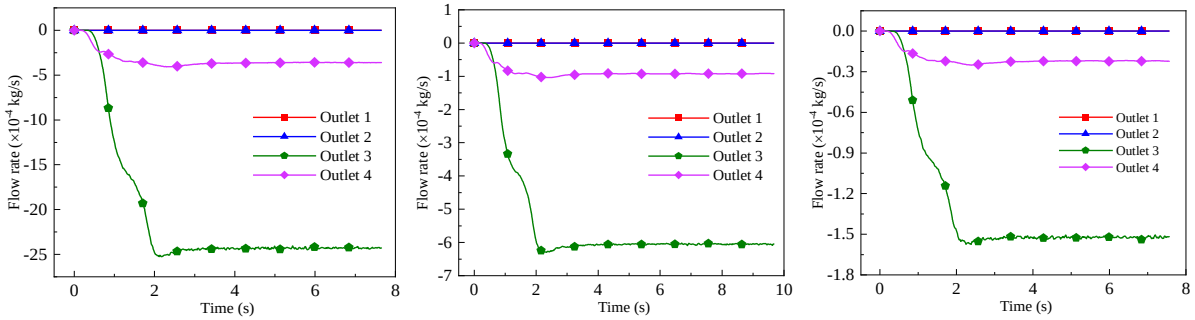

(a) Case 1 (b) Case 2 (c) Case 3

Fig. 8 Leakage gas outlet flow rate diagrams in three cases.

According to the above analysis, the value of the outlet flow rate when reaching a stable level is proportional to the leakage intensity. Namely, when the leakage intensity increases by K times, the outlet flow rate will also increase by K times.

4 Conclusions

Based on the actual situation in the power plant, this paper developed a three-dimensional physical model of the condenser. The model considers the complex tube bundle area in the condenser as porous media. The flow field inside the tube bundle and the leakage gas transport under various operating conditions are simulated. The following conclusions can be drawn:

(1) The extraction of leakage gas primarily depends on the centripetal pressure gradient within the cooling area of the tube bundle. Driven by this centripetal pressure gradient, leakage gas can flow out from the extraction port. Increasing the operating load, improving the circulating water temperature, or reducing the amount of circulating water can enhance the centripetal pressure gradient to quickly stabilize the outlet flow rate.

(2) There are two leakage gas transport forms: flow and diffusion. When there is sufficient centripetal pressure, leakage gas will flow out along with the steam through the extraction port. When the centripetal pressure is insufficient, the leakage gas will enrich until it reaches a concentration level that allows diffusion towards the outlet due to the concentration difference.

(3) The leakage gas intensity only positively affects the outlet flow rate. And stable outlet flow rate value is proportional to the leakage intensity. Changing the leakage gas intensity does not affect the trend or time required for the outlet flow rate to reach stability.

(4) The deviation of the mass flow rate decreases with the mesh quantity increasing, which is less than 2% when the mesh quantity is over 638228. The deviation between simulated and actual values of the two parameters is less than 5%, which reveals the good agreement between numerical calculation and actual work conditions.

The above conclusions provide valuable insights for employees and researchers for analyzing leak point information such as the leak point size, the position where the leak occurs, and the amount of the leakage gas, to improve the measurement method. Furthermore, altering detected gas may yield positive effects on the measurement techniques and results, which need to be studied in future.

Nomenclature

C_A	Cooling tube heat-transfer area, m^2
C_V	Control body thermal volume, m^3
c_a	Diffusion coefficient of Helium, m^2/s
F_x, F_y, F_y	Flow resistance of the mixed gas in the x, y, and z directions, Pa
$\dot{m}$	Condensation rate of steam per unit volume locally, W/[kg/(m^2· s)]
M_a	Helium mass sink
p	Condenser pressure, Pa
R	Steam gas constant, J/(mol· K)
R_{tot}	Total thermal resistance from the steam side to the waterside, K/W
T	Stream temperature, K
Δt_m	Logarithmic average temperature difference, ℃
U_p	Magnitude of velocity, m/s
u, v, w	Flow velocities in the x, y, and z directions, m/s
x_a	Mass concentration of leakage gas
Greek symbols	
β	Porous media model porosity
γ	Latent heat of the local steam condensation, J
ρ	Steam density, kg/m^3
μ	Dynamic viscosity, kg/(m· s)
ξ	Dimensionless parameter related to the distribution of the bundle structure and the direction of the gas flow

Acknowledgements

This work was supported by the National Natural Science Foundation of China (U1905216), the Key Scientific and Technological Project of Henan Province (162102310152), and the Joint Research Project of Industry of China (H23-043). The computer simulation was supported by the high-performance computing platform of Henan Polytechnic University.

References

[1] Zeng, H., Z. Li, Numerical study of a power plant condenser tube arrangement, Applied Thermal Engineering, 40 (2012), pp. 294-303, DOI: 10.1016/j.applthermaleng.2012.02.028

[2] Ahmadi, G.R.,D. Toghraie, Energy and exergy analysis of Montazeri steam power plant in Iran, Renewable and Sustainable Energy Reviews, 56 (2016), pp. 454-463, DOI: 10.1016/j.rser.2015.11.074

[3] Mathews, I., et al., A simulation-based prediction model for coal-fired power plant condenser maintenance, Applied Thermal Engineering, 174 (2020), p. 115294, DOI: 10.1016/j.applthermaleng.2020.115294
[4] Medica-Viola, V., et al., Numerical model for on-condition monitoring of condenser in coal-fired power plants, International Journal of Heat and Mass Transfer, 117 (2018), pp. 912-923, DOI: 10.1016/j.ijheatmasstransfer.2017.10.047
[5] Roy, R., et al., A computational model of a power plant steam condenser, J. Energy Resour. Technol., 123 (2001), 1, pp. 81-91, DOI: 10.1115/1.1348336
[6] Prabu, S.S., et al., Experimental study on performance of steam condenser in 600 MW singareni thermal power plant, International Journal of Mechanical Engineering and Technology (IJMET) Vol, 9 (2018), 3, pp. 1095-1106
[7] Moore, W., Power station condensers their design and failure modes, Materials at High Temperatures, 34 (2017), 5-6, pp. 407-414, DOI: 10.1080/09603409.2017.1370191
[8] Rao, T.S., S. Bera, Protective layer dissolution by chlorine and corrosion of aluminum brass condenser tubes of a nuclear power plant, Engineering Failure Analysis, 123 (2021), p. 105307, DOI: 10.1016/j.engfailanal.2021.105307
[9] Lee, J.C., et al., Pipe leakage detection using ultrasonic acoustic signals, Sensors and Actuators A: Physical, 349 (2023), DOI: 10.1016/j.sna.2022.114061
[10] Golovin, V., et al., Determination of the life cycle of heat-exchange tubes of vapor condensers on the basis of statistical analysis of local pitting corrosion according to data of eddy current testing, Protection of Metals and Physical Chemistry of Surfaces, 54 (2018), pp. 1221-1232, DOI: 10.1134/S2070205118060138
[11] Yokell, S., Pressure Testing Feedwater Heaters and Power Plant Auxiliary Heat Exchangers, Journal of Pressure Vessel Technology, 133 (2011), 5, DOI: 10.1115/1.4003468
[12] Li, J., et al., On-line fouling monitoring model of condenser in coal-fired power plants, Applied Thermal Engineering, 104 (2016), pp. 628-635, DOI: 10.1016/j.applthermaleng.2016.04.131
[13] Jawwad, A.K.A.,I. Mohamed, The combined effects of surface texture, flow patterns and water chemistry on corrosion mechanisms of stainless steel condenser tubes, Engineering Failure Analysis, 109 (2020), p. 104390, DOI: 10.1016/j.engfailanal.2020.104390
[14] Leng, Z., et al., Research on improving the system sensitivity for Hot Helium Leak Test, Fusion Engineering and Design, 188 (2023), p. 113422, DOI: 10.1016/j.fusengdes.2023.113422
[15] Wang, K., et al., China's progress on hot helium leak test of ITER shield blocks, Fusion Engineering and Design, 193 (2023), p. 113669, DOI: 10.1016/j.fusengdes.2023.113669
[16] Juan, D.,Z. Hai-Tao, Numerical simulation of a plate-fin heat exchanger with offset fins using porous media approach, Heat and Mass Transfer, 54 (2017), 3, pp. 745-755, DOI: 10.1007/s00231-017-2168-3
[17] Abe, S., et al., Density stratification breakup by a vertical jet: Experimental and numerical investigation on the effect of dynamic change of turbulent schmidt number,

Nuclear Engineering and Design, 368 (2020), p. 110785, DOI: 10.1016/j.nucengdes.2020.110785
[18] Shin, D., et al., Development of the thermal performance model using temperature gradient analysis for optimized design of steam surface condenser, International Journal of Heat and Mass Transfer, 163 (2020), p. 120411, DOI: 10.1016/j.ijheatmasstransfer.2020.120411
[19] Versteeg, H.K.,W. Malalasekera, An introduction to computational fluid dynamics: the finite volume method. Pearson education, 2007.
[20] Yang, R.J.,W.J. Luo, Turbine blade heat transfer prediction in flow transition using k-omega two-equation model, Journal of Thermophysics & Heat Transfer, 10 (1996), 4, pp. 613-620, DOI: 10.2514/3.837
[21] Zhang, C., et al., The Numerical and Experimental Study of a Power Plant Condenser, ASME Journal of Heat and Mass Transfer, 115 (1993), 2, pp. 435-445, DOI: 10.1115/1.2910696
[22] Davies, W.A., et al., Heat transfer and flow regimes in large flattened-tube steam condensers, Applied Thermal Engineering, 148 (2019), pp. 722-733, DOI: 10.1016/j.applthermaleng.2018.11.079
[23] Cavalcanti, L.L.F., et al., Determination of CO2 solubility in Perna perna mussel and analysis of the suitability of the ideal and non-ideal gas models, Chemical Thermodynamics and Thermal Analysis, 7 (2022), p. 100075, DOI: 10.1016/j.ctta.2022.100075
[24] Ahn, S.-H., et al., Unsteady prediction of cavitating flow around a three dimensional hydrofoil by using a modified RNG k-ε model, Ocean Engineering, 158 (2018), pp. 275-285, DOI: 10.1016/j.oceaneng.2018.04.005

Received: 24.07.2023.
Revised: 14.12.2023.
Accepted: 16.01.2024.